RSC Advances

PAPER

View Article Online
View Journal | View Issue

Cite this: *RSC Adv.*, 2025, **15**, 16076

Monolayer CuBr-based gas sensor to detect habitat and industry-relevant molecules with high sensitivity and selectivity: a first-principles study

Shamiala Pervaiz,[a] M. Usman Saeed,[a] Hazrat Ali,[a] Y. Saeed,*[a] Aamir Khan[b] and Yousef Mohammed Alanazi[c]

The adsorption characteristics of different environmental gas molecules such as HF, CO, CO_2, SO_2, H_2S, NH_3, NO and NO_2 on the surface of a CuBr monolayer have been studied using DFT+*U* calculations with Grimme scheme DFT-D2 for accurate description of the long-range interactions (van der Waals). Our findings indicate that the CuBr monolayer (ML) exhibits high sensitivity to CO, SO_2, H_2S, NH_3, NO and NO_2, as evidenced by their strong adsorption energies and significant charge transfer. In contrast, HF and CO_2 molecules show weak adsorption on the CuBr ML, due to their low adsorption energies and minimal charge transfer. High diffusion energy barriers for gas molecules (CO, CO_2, NH_3 and NO_2) indicate that they are less mobile and tend to remain stable at their adsorption sites. Conversely, low diffusion energy barriers (HF, SO_2, H_2S and NO) suggest that a lesser amount of energy needs to be expended and gases can move easily across the surface of the substrate. The band structure and partial density of states calculations reveal that the electronic properties of the CuBr ML are altered due to the contributions of the orbitals of the gas molecules (C-p and O-p of CO, F-p of HF, O-p of CO_2, S-p of H_2S, N-p of NH_3, S-p and O-p of SO_2, N-p and O-p of NO and NO_2) and CuBr ML (Cu-p, Cu-d, Br-p). The charge density difference and Bader charge analysis indicate that the gas molecules (CO, HF, SO_2, CO_2, NO and NO_2) either act as charge acceptors or donors (H_2S and NH_3). The work function variations of the CuBr ML before and after adsorption and significant changes in the conductivity verify the high sensitivity of CO, SO_2, H_2S, NH_3, NO and NO_2 with the CuBr ML. The band gap variations (before and after adsorption) are small for HF, CO, CO_2, H_2S and NH_3 whereas large variations in band gap for SO_2, NO and NO_2 reveal that the CuBr ML is quite selective to these three gases. The recovery time for gas molecules desorption from CuBr ML is reduced to a reasonable recovery time by increasing the temperature from ambient to 500 K with UV exposure. Thus our theoretical results indicate that the CuBr ML is a promising candidate as a gas sensor for sensing applications of CO, SO_2, H_2S, NH_3 NO and NO_2 with high sensitivity and selectivity.

Received 8th September 2024
Accepted 9th April 2025

DOI: 10.1039/d4ra06492e

rsc.li/rsc-advances

1. Introduction

Two-dimensional (2D) materials have garnered a great deal of attention because of their fascinating electrical, chemical and physical characteristics, their incredible thinness, availability of active sites, large surface-to-volume ratio, suitable carrier density and other appealing quantum properties.[1–3] 2D nano devices have applications in many fields.[4,5] 2D materials are highly promising for use as high-efficiency nanosensors as the gas molecule's adsorption on the surface of a 2D nanomaterial results in a significant change in the electrical conductivity with little change in the carrier concentration.[6,7] Emission of hazardous and toxic gases have raised severe concerns about the quality and quantity regulation of these harmful gases in both indoor and outdoor areas. Exposure to these harmful gases has negative impacts on the ecosystem and human health.[8,9] Thus, a significant amount of work has been done for the precise identification and detection of harmful gases in the environment.[10] Gas sensors are devices that use materials that sense gases in the surrounding air to determine the composition and concentration of gases. High sensitivity, high selectivity, performance stability, fast response, low working temperature and low power consumption are the fundamental standards and performance metrics for a gas sensor.[11] Unfortunately, a few intrinsic drawbacks of common 2D materials, like graphene's zero band gap,[12] MoS_2's low carrier mobility and

[a]*Department of Physics, Abbottabad University of Science and Technology, Abbottabad, KPK, Pakistan. E-mail: yasir.saeed@kaust.edu.sa; yasirsaeedphy@aust.edu.pk; Tel: +(92)-3454041865*

[b]*Shenzhen Key Laboratory of Laser Engineering, College of Physics and Optical Engineering, Shenzhen University, Shenzhen 518060, China*

[c]*College of Engineering, Chemical Engineering Department, King Saud University, Riyadh, Saudi Arabia*

α-p's low chemical stability[13] severely restrict their widespread application. This has spurred ongoing research into finding additional 2D materials with characteristics that could result in particular enhanced performance. The graphene family,[14] 2D metal oxides,[15] transition metal dichalcogenides (TMDCs)[16] such as WS_2,[17] WSe_2,[18] MoS_2,[19] MXenes,[20] single element materials, such as black phosphorous,[21] arsenene,[22] antimonene[23] and so on, are examples of emerging 2D materials used in gas sensing.

2D metal halide monolayers can be made by simply mechanically exfoliating 3D bulk phases. Among the different metal halides, 2D semiconductor cuprous bromide (CuBr) possesses a variety of applications in various fields. It is a very promising material for usage in UV photodetectors, photocatalysis, light-emitting devices and quantum cutting.[24,25] It belongs to the group of tetrahedrally coordinated binary compounds. These compounds are of great interest to researchers and those who study the fundamentals of semiconductor physics. Several groups have explored the fundamental structures, electrical characteristics and stability for copper(I/II) bromide surfaces using DFT.[25,26] Single-layer CuBr has a cleavage energy value of 0.291 J m^{-2} (ref. 26) which is less than graphene's (0.37 J m^{-2}).[27] This suggests that the CuBr monolayer can be easily manufactured by mechanical exfoliation. Calculations of the phonon spectrum are used to assess the dynamic stability of the CuBr ML.[26] The absence of an imaginary mode in the CuBr monolayer implies that it is dynamically stable and could potentially exist as an independent 2D crystal and it is also thermally and mechanically stable with a formation energy of −0.27 eV.[26] The electron mobility (∼1153.54 cm^2 V^{-1} s^{-1}) of the CuBr ML[26] is similar to phosphorene (∼1000 cm^2 V^{-1} s^{-1})[28] and greater than other 2D semiconductors, including MoS_2 (∼200 cm^2 V^{-1} s^{-1})[29] and BN (∼487 cm^2 V^{-1} s^{-1}).[30] The CuBr ML possesses a band gap of 3.198 eV and Γ(0, 0, 0) is the location of the valence band maximum and conduction band minimum.[26]

Pervaiz *et al.*[31] studied in detail the adsorption of CO and HF gas molecules on a CuCl ML using the DFT+*U* method. Different parameters like adsorption energy, band gap energy, nudged elastic band, charge density difference, work function, conductivity and recovery time were calculated to study the sensitivity and selectivity of the CuCl ML for these gases. Likewise previous research studies show adsorption of toxic gas molecules on various materials including InN, phosphorene, Janus Te_2Se, graphene (doped), ZnS, Ti-doped hBN, TMDCs, $MoSi_2N_4$, graphene, Ti_2CO_2, arsenene and defective tellurine.[32–43]

In this research work, founded on computations from first principles, we inclusively investigated a wide range of gas molecules on the CuBr ML, including combustible (CO, H_2S, NH_3), non-combustible (HF), inert gases (CO_2, SO_2) and oxidizers (NO, NO_2) which have not been presented before. The properties of the adsorption system (gas–CuBr), such as the adsorption energy (E_{ads}), distance (*d*, between gas molecule and ML), charge shifted (ΔQ), total and partial density of states (DOS/PDOS), band gap energy, work function, conductivity and recovery time were calculated to investigate the sensitivity and selectivity of a CuBr sensor with these toxic gas molecules. The nudged elastic band (NEB) model and the charge density difference (CDD) were also used to investigate the potential adsorption mechanism and interaction. The findings show that the electronic and magnetic characteristics of the CuBr ML are influenced by the adsorption of various molecules, which makes it suitable to use as a gas sensing material. As far as we are aware, there hasn't been any research on how various molecules adsorb on the CuBr monolayer or how this affects the monolayer's characteristics. Therefore, this paper's goal is to fill in the knowledge gap in this area.

2. Computational details

The quantum espresso package[44] is the *ab initio* code utilized in our research work for structural optimization and electronic properties calculation. To relax the structures, the plane-wave basis set using generalized gradient approximation, as indicated by the Perdew–Burke–Ernzerhof functional,[45] is applied. Ultra-soft pseudo-potentials[46] were used to express the valence electrons and ionic core interaction. Furthermore, for a precise representation of van der Waals interactions between the monolayer and gas molecules, the Grimme scheme DFT-D2 is applied[47] as DFT produced accurate results in the previous studies.[48–51] The Coulomb repulsion interaction between the electrons in the Cu:3d and Br:4p orbitals is considered utilizing the DFT+*U* approach, which is also utilized for the correction of self-interaction error in the s, p, d, and f states.[52] So, the PBE functional includes the Hubbard parameter (*U*),[53,54] obtained *via* the ACBN0 technique[55] chosen as *U* (Cu:3d) = 6.3 eV and *U* (Br:4p) = 6.3 eV, in accordance with Mehta *et al.*[56]

A CuBr monolayer consisting of 18 atoms (nine Cu and nine Br atoms) is utilized, with a 3 × 3 × 1 supercell having lattice constants of $a = b = 12.150$ Å. A vacuum of 20 Å is set in order to separate neighboring repeated images of the supercell. Each atom is subjected to a force of less than 0.005 eV $Å^{-1}$ for structural relaxation. A cutoff of 650 eV in kinetic energy for the wavefunction and 10^{-8} eV energy convergence is employed. A 4 × 4 × 1 *k*-mesh is taken to depict the first Brillouin zone using the Monkhorst–Pack technique.[53] For the precision of electronic computations, Brillouin zone sampling employs a denser *k*-mesh of 12 × 12 × 1.

Bader charge analysis is applied to look into the charge transformation between the CuBr ML and gas molecule.[54] The following relationship is utilized to assess the gas molecule's adsorption phenomenon strength on the CuBr ML:[31]

$$E_{ads} = E_{total} - (E_{CuBr} + E_{gas\ molecule}) \quad (1)$$

where E_{ads} is adsorption energy, E_{total} is the combined system energy (gas–CuBr), E_{CuBr} is the pristine CuBr ML's energy and $E_{gas\ molecule}$ is the gaseous molecule energy.

The climbing image nudged elastic band approach is employed for tracing the lowest energy pathway (between the beginning and final coordinates) during adsorption of molecules. The transition state search is done for this reason. One can find the DEB as follows:[31]

$$E_{DEB} = E_{TS} - E_{IS} \quad (2)$$

where E_{IS} denotes the initial state energy and E_{TS}, the transition state energy (final transition state in the case of more than one transition).

The charge density difference (CDD) for the monolayer–molecule systems is determined using the following formula:[32]

$$\Delta\rho = \rho_{total}(r) - \rho_{CuBr}(r) - \rho_{gas}(r) \quad (3)$$

where the charge distribution of the gas-adsorbed CuBr ML is represented by $\rho_{total}(r)$. In the absence of gas adsorption, the charge distribution of the free CuBr ML is $\rho_{CuBr}(r)$, and the free gas molecule's distribution of charges is represented by $\rho_{gas}(r)$. The gas molecule and the free CuBr have the same coordinates as when they are adsorbed.

The work function is the minimum energy required for the ejection of electrons from the Fermi level to infinity for the adsorbed gas, which can be computed as:[31]

$$\phi = V(\phi) - E_{Fermi} \quad (4)$$

where ϕ stands for work function, $V(\phi)$ for electrostatic potential and E_{Fermi} for the Fermi energy of the CuBr ML.

The equation below relates to the conductivity of the CuBr ML, which varies as a result of the gas molecules' adsorption phenomena:[55]

$$\sigma = A\, e^{-E_g/k_B T} \quad (5)$$

In this case, σ stands for electrical conductivity, A is the proportionality constant, T is absolute temperature, E_g denotes the band gap energy and k_B denotes the Boltzmann constant. The sensitivity can be defined by the change in conductivity, which can be written as:[55]

$$\frac{\delta\sigma}{\sigma} = \frac{\exp\left(-\frac{E_g(\mathrm{CuBr+gas})}{2k_B T}\right) - \exp\left(-\frac{E_g(\mathrm{CuBr})}{2k_B T}\right)}{\exp\left(-\frac{E_g(\mathrm{CuBr})}{2k_B T}\right)} \quad (6)$$

In order to evaluate the reusability of a gas sensor, its recovery time is calculated using the following equation:[31]

$$\tau = {v_0}^{-1}\, e^{\frac{-E_{ads}}{k_B T}} \quad (7)$$

In this case E_{ads} stands for adsorption energy, v_0 ($= 10^{12}$ s^{-1})[55] for the frequency of the molecular attempt, and k_B ($= 8.617 \times 10^{-5}$ eV K^{-1}) is the Boltzmann constant.

3. Results and discussion

The dynamic stability of the CuBr ML has been evaluated by examining the phonon dispersion plot, as illustrated in Fig. 1. Nearly all of the modes in the phonon dispersion plot of CuBr show positive frequency in the range of the Γ–Γ high symmetry k-point, which is in accordance with the previous theoretical research on the CuBr ML,[26] so it is implied that the CuBr monolayer is dynamically stable and may exist as an independent 2D crystal as it does not exhibit an imaginary mode.

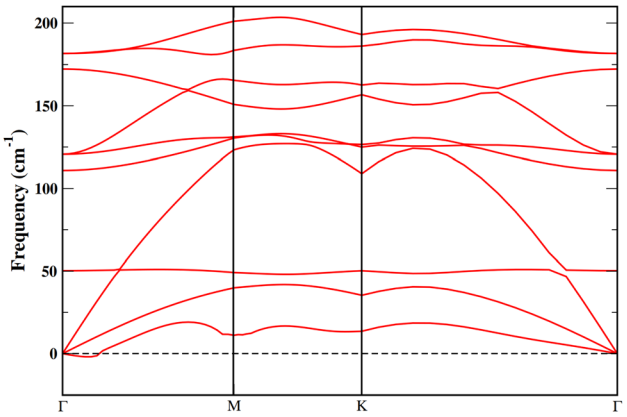

Fig. 1 Phonon dispersion spectrum of the CuBr monolayer.

The different gas molecules are initially positioned above the CuBr ML with varying orientations for determining the most energetically stable configurations of adsorption with the lowest energy. The gaseous molecules HF, CO, CO_2, SO_2, H_2S, NH_3, NO and NO_2 were initially positioned at a distance of 3.0 Å above the adsorption sites and the system was completely relaxed after adsorption. For the gas molecules' adsorption on the CuBr ML, we first took into consideration a number of typical adsorption sites as shown in Fig. 2 namely, center (above hexagon center), Cu (above Cu atom), Br (above Br atom), and bridge (above Cu–Br link). Additionally on the CuBr surface, many typical orientations of gas molecules are also taken into consideration. As an example of SO_2 molecule adsorption, the SO_2 molecule is first positioned vertically (CuBr↔O–SO, and CuBr↔O_2–S) or in parallel (CuBr↔O_2–S, and CuBr↔S–O_2) on the surface of the CuBr ML for each and every adsorption site under study. So all the orientations of the SO_2 molecule are taken into account. It is clear that distinct gas molecules prefer different adsorption sites and configurations within the same substrate. Furthermore, it is evident that several gas molecules, including CO, CO_2, SO_2, NH_3, H_2, NO and NO_2, caused buckling effects and structural deformation, which are produced in the monolayer due to adsorption of these gas molecules compared to the pristine CuBr monolayer as shown in Fig. 2. It is also observed that after adsorption, variation in the bond length and bond angle of the gas molecules has occurred as Fig. 3 shows the configurations of the gas molecules after adsorption.

Table 1 lists the adsorption energy values (E_{ads}) on different sites (center, Cu, Br and bridge), D, closest distance (between gas molecule and the CuBr ML), and Q, total charge transfer between the CuBr ML and gas molecules. For most of the adsorption systems of CuBr with gas molecules (HF, CO, CO_2, SO_2, NO, NO_2), it is concluded that the adsorption energy absolute values rise as the distance of adsorbed molecule decreases. Eqn (1) is used for the calculation of adsorption energy. The charge transfer between the gas molecules and the CuBr ML is provided by Bader charge analysis.[54]

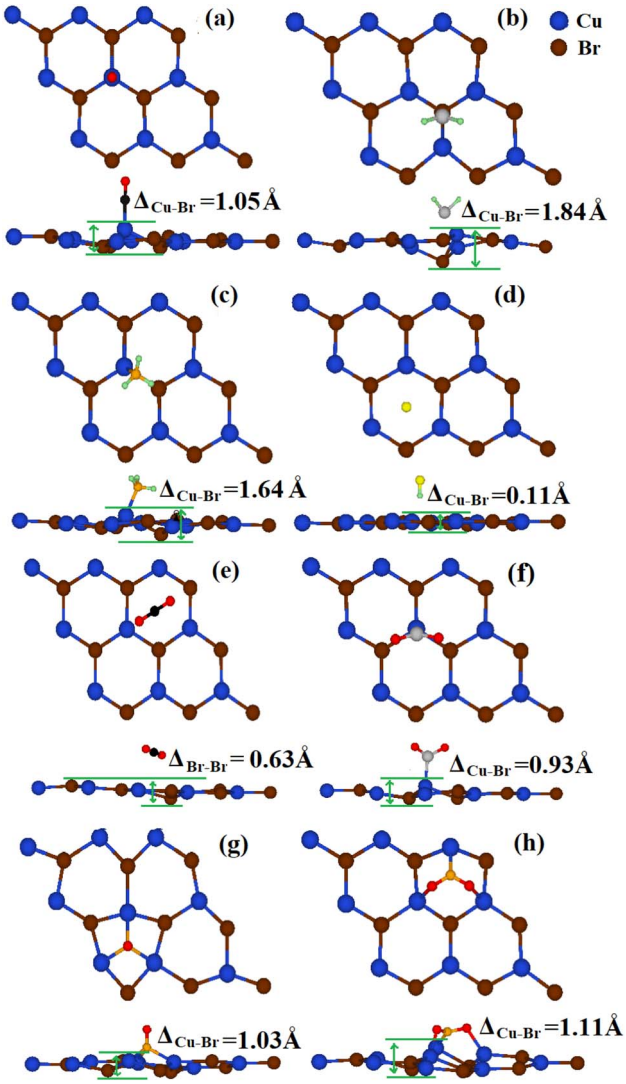

Fig. 2 Top and side views (most favorable configurations with different buckling heights for adsorption on the CuBr ML) of (a) CO, (b) H_2S, (c) NH_3, (d) HF, (e) CO_2, (f) SO_2, (g) NO and (h) NO_2. Green, yellow, red, black, gray and orange balls represent H, F, O, C, S, and N atoms respectively.

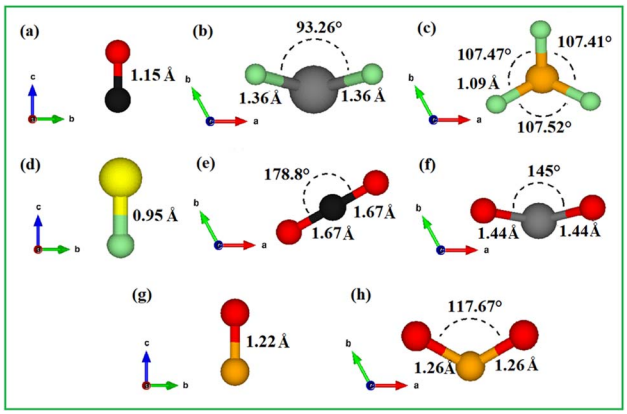

Fig. 3 Configuration of adsorbed gas molecules of (a) CO, (b) H_2S, (c) NH_3, (d) HF, (e) CO_2, (f) SO_2, (g) NO and (h) NO_2 on the CuBr ML. Green, yellow, red, black, gray and orange balls represent H, F, O, C, S, and N atoms respectively.

In the case of combustible gases, CO, H_2S and NH_3, all these gases show strong adsorption on the CuBr monolayer having E_{ads} absolute values of 1.285, 1.172 and 1.287 eV with charge transfer of $-0.111|e|$, $0.027|e|$ and $0.117|e|$ respectively. These combustible gas molecules have different optimal sites on the CuBr ML as shown in Table 1. CO and NH_3 molecules have small adsorption distances of 1.796 and 1.850 Å respectively, whereas the adsorption distance for H_2S is 2.203 Å. All the three combustible gas molecules show physisorption on CuBr on the basis of E_{ads}, adsorption distance and small charge transfer values. These results demonstrate that the CuBr ML exhibits significant potential in the sensing of these combustible gases. Consequently it is evaluated that the CuBr ML shows very good adsorption for these combustible gases when comparing with E_{ads} values on other 2D materials which have been previously studied, like InN (for CO, H_2S and NH_3), phosphorene (for CO and NH_3), Janus Te_2Se (for CO, H_2S and NH_3), graphene (for CO and NH_3), ZnS monolayer (for CO) as well as pristine hBN (for CO, H_2S) and Ti doped hBN (for CO).[32–37]

For the non-combustible HF gas molecule, the center and bridge sites are the optimal configurations on the CuBr ML as the adsorption energies (−0.222 and −0.229 eV) on these sites are not much different with small $Q = -0.032$ and $-0.056|e|$ respectively. The adsorption distances for HF molecules on center and bridge sites are 2.183 and 1.648 Å respectively. It is observed that there is very little interaction between the CuBr and the HF molecule. The HF molecule also shows physisorption on CuBr due to small E_{ads} and charge transfer values.

In the case of inert gases SO_2 and CO_2, a good interaction is observed for the SO_2 gas molecule as compared to CO_2 (weak adsorption) with E_{ads} value of −0.632 and −0.277 eV on Cu sites respectively. Both these inert gas molecules show different adsorption behaviour on different sites as shown in Table 1. Similarly for the SO_2 molecule more charge transfer is observed ($-0.158|e|$) as obvious from its greater adsorption energy compared with the small charge transfer for CO_2 ($-0.014|e|$) with adsorption distances of 2.071 and 2.762 Å respectively. These two inert gas molecules also show physisorption on the CuBr ML on the basis of E_{ads} value, adsorption distance and small charge transfer values. The CuBr ML showed a significantly good adsorption energy value for SO_2 and CO_2 molecules when comparing with E_{ads} values on other substrates like Janus Te_2Se-based ML (for SO_2),[34] hBN (for CO_2),[37] $MoSi_2N_4$ (for SO_2 and CO_2),[39] pristine graphene (for CO_2),[40] Ti_2CO_2 (for CO_2)[41] and pristine arsenene (for SO_2).[42]

Regarding the adsorption of oxidizer gases NO and NO_2, their nitrogen end, often known as the nitro configuration, is attached to the monolayer surface similar to the previous studies.[41] This nitro configuration with the center site is the most optimal site for both the molecules. Both oxidizer molecules show strong adsorption with E_{ads} values of about −0.852 and −1.754 eV with small adsorption distances of 0.952 and 1.233 Å respectively. It is also observed that a huge charge of

Table 1 Adsorption sites, adsorption energy (E_{ads}), adsorption distance (D), charge transfer (Q) and molecular nature (donor/acceptor) on the CuBr ML for CO, H_2S, NH_3, HF, SO_2, CO_2 NO and NO_2

Model	Site	E_{ads} (eV)	D (Å)	Q (e^-)	Molecule on CuBr
CO	Bridge	−1.284	1.798	−0.097	Donor
	Cu	−1.285	1.796	−0.111	
	Br	−0.136	3.519	−0.014	
	Center	−0.262	2.111	−0.063	
H_2S	Bridge	−1.037	3.326	0.098	Acceptor
	Cu	−1.124	3.252	0.111	
	Br	−1.172	2.203	0.027	
	Center	−0.859	2.747	0.047	
NH_3	Bridge	−1.287	1.850	0.117	Acceptor
	Cu	−1.280	1.901	0.115	
	Br	−0.363	3.343	0.012	
	Center	−0.332	2.578	0.019	
HF	Bridge	−0.222	2.183	−0.032	Donor
	Cu	−0.075	2.266	−0.060	
	Br	−0.188	2.205	−0.059	
	Center	−0.229	1.648	−0.056	
SO_2	Bridge	−0.591	2.140	−0.188	Donor
	Cu	−0.632	2.071	−0.158	
	Br	−0.297	3.335	−0.110	
	Center	−0.316	2.751	−0.158	
CO_2	Bridge	−0.248	3.108	−0.040	Donor
	Cu	−0.277	3.294	−0.034	
	Br	−0.253	3.106	−0.042	
	Center	−0.224	2.762	−0.014	
NO	Bridge	−0.739	1.805	−0.261	Donor
	Cu	−0.791	1.775	−0.244	
	Br	−0.187	3.231	−0.077	
	Center	−0.852	0.952	−0.528	
NO_2	Bridge	−0.965	1.930	−0.521	Donor
	Cu	−0.850	1.942	−0.518	
	Br	−1.429	1.910	−0.519	
	Center	−1.754	1.233	−0.812	

about $-0.528|e|$ and $-0.812|e|$ is transferred from the CuBr ML to the NO and NO_2 molecules respectively. Both the gas molecules show chemisorption on the CuBr ML on the basis of large E_{ads}, small adsorption distance and large charge transfer values. It is evaluated that CuBr shows good adsorption affinity for NO and NO_2 molecules as compared to other 2D monolayers like InN (for both NO and NO_2),[32] Janus Te_2Se (for both NO and NO_2),[34] graphene (for NO and NO_2),[35] pristine hBN (for NO),[37] tellurine (for NO and NO_2)[43] and phosphorene (for NO_2).[33]

The adsorption of all gaseous molecules on the CuBr ML is energy favourable and occurs through an exothermic process, as indicated by the negative sign of the adsorption energy. Fig. 4 gives a comparison of the adsorption energy values of the different molecules (HF, CO, CO_2, SO_2, H_2S, NH_3, NO and NO_2) at the most stable site (center, Cu, Br, bridge).

Moreover a transition state search is executed to gain more understanding of the optimal configuration. The NEB

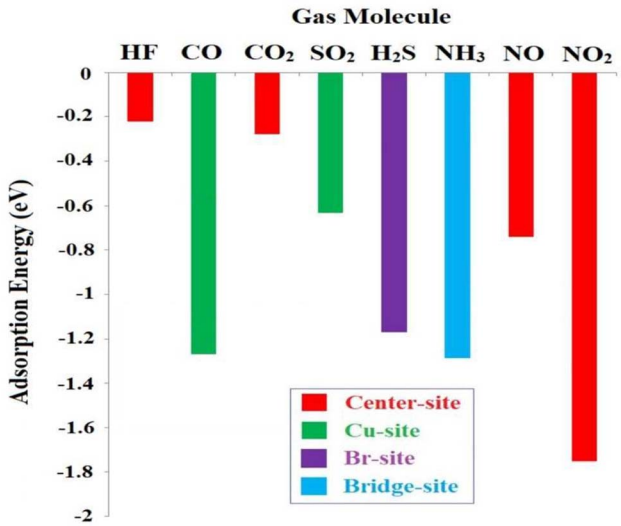

Fig. 4 Comparison of adsorption energy values of different molecules on the CuBr ML at the most stable site.

calculations are used to identify the least energy path between the reactants and products. The results of different gas molecules are displayed in Fig. 5. The accuracy of the adsorption energy calculations is confirmed by the reaction path's energy relationship, which demonstrates that the best location for adsorption is indeed the site with the lowest energy. In NEB calculations, the Initial State (IS), Transition State (TS), and Final State (FS) are key points along the minimum Energy Path, which describes the reaction or adsorption process and scenarios of how the gases move on the CuBr surface. These states are used to determine the diffusion energy barrier (DEB) for adsorption of gas molecules on the CuBr ML. The IS state is the starting configuration where the adsorbate gas molecule is positioned at an initial adsorption site before migration. In this state, the interaction between the molecule and the surface is minimal. As the system (CuBr–gas) progresses along the reaction pathway, it reaches the TS, which corresponds to the highest energy point along the minimum Energy Path and represents the reaction or diffusion barrier. At the TS, partial bond formation occur, and the gas molecule is in an unstable or metastable configuration. This state is crucial for determining the DEB, which is the energy difference between the TS and IS as given in eqn (2). Finally, the system reaches the FS, which represents the most stable configuration after the transition. At the FS, the gas molecule is fully adsorbed at a preferred site on the surface. The total energy of the system at the FS is lower than or comparable to the IS, indicating a more stable configuration. The adsorption energy at this state is minimized, confirming strong interactions between the gas molecule and the CuBr ML. The NEB method interpolates between the IS and FS through the TS using "images" to capture intermediate states and is plotted when gas molecules are migrating from one optimal site to another optimal site on the monolayer surface.[56,57] For CO and CO_2 adsorption on the CuBr monolayer, the most stable optimal adsorption site (minimum energy site)

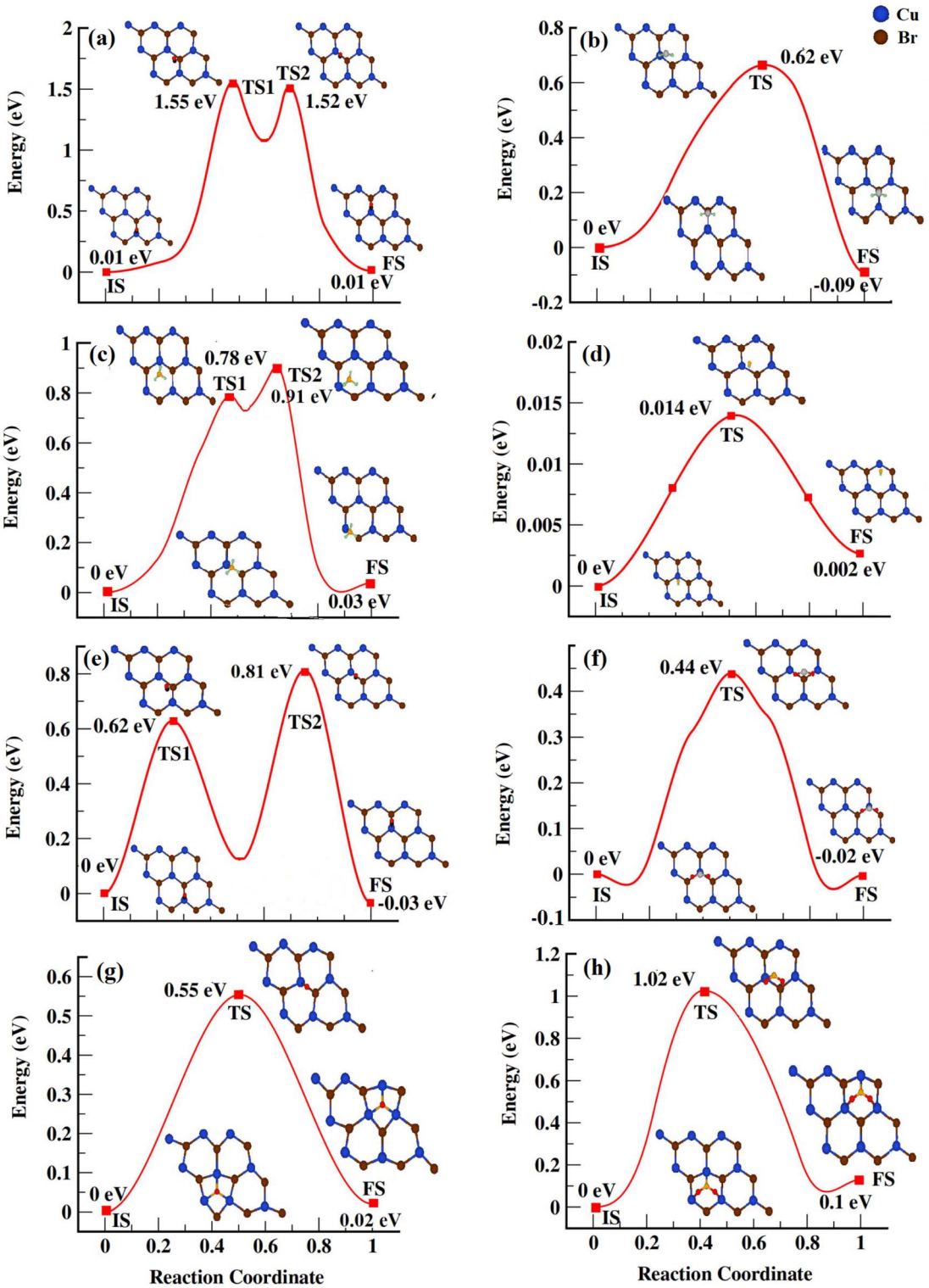

Fig. 5 Diffusion energy barrier with diffusion pathway and configurations of initial, transition and final states of (a) CO, (b) H_2S, (c) NH_3, (d) HF, (e) CO_2, (f) SO_2, (g) NO and (h) NO_2. Green, yellow, red, black, gray and orange balls represent H, F, O, C, S, and N atoms respectively.

is the Cu site, shown in Table 1, which is designated as the IS. The neighboring Cu site is considered the FS, while the transition states (TS1 and TS2) occur *via* the Br (or near Br) site and the bridge site, as depicted in Fig. 5. Our calculations indicate that the Cu–Br–bridge–Cu pathway is the most favorable diffusion route of minimum energy for CO and CO_2 adsorption on the CuBr ML. Similarly, for H_2S adsorption, the molecule migrates from the Br site (IS), which is the optimal site to the

adjacent Br site (FS) through the Cu site as the TS, encountering a diffusion barrier of 0.62 eV given in Table 2. For NH_3 adsorption, the IS is the bridge site, the transition states (TS1 and TS2) occur at the center site, and the FS returns to the bridge site. For SO_2, the IS, TS and FS states are Cu, Br and Cu respectively. Similarly, for HF, NO, and NO_2 adsorption on the CuBr monolayer, the center site is identified as the most stable adsorption site and is designated as the IS. The neighboring center site serves as the FS, with the TS occurring *via* the bridge site. Our calculations verify that the center–bridge–center route is the most preferred diffusion path with the least energy for these gas molecules. Therefore by accurately defining the IS, TS and FS and using interpolated images between them, NEB calculations provide an accurate estimation of the energy barrier, adsorption stability, and reaction kinetics for surface processes on the CuBr ML.

There are two observed transition states in the cases of CO, CO_2 and NH_3 designated as TS1 and TS2, with TS2 being used for DEB calculations. An intermediate stage between TS1 and TS2 is also observed. During the course of motion of gas molecules from the starting state to the optimal final state, an intermediate state exists, which is an unstable reaction in adsorption. Eqn (2) is used to compute the DEB by considering Fig. 5, where the DEB values for CO, H_2, NH_3, HF, CO_2, SO_2, NO and NO_2 are given in Table 2. The higher value of the energy barrier for CO, CO_2, NH_3 and NO_2 when these molecules are migrating from one optimal site to another suggests that these gases are less mobile and tend to remain stable at their adsorption sites, while the small value of DEB for HF, SO_2, H_2S and NO indicates that a lesser amount of energy needs to be expended and these gases can move easily across the surface of the CuBr ML as according to the previous study on DEB calculations.[58]

To evaluate the impact of gas adsorption on the electronic properties of the CuBr ML in more detail, we examined the total DOS, PDOS and band structures as shown in Fig. 6 and 7. These calculations reveal that the electronic properties of the CuBr monolayer are altered due to the orbital contributions from the gas molecules near the Fermi level as compared to pristine CuBr ML. The band gap energies of the CuBr ML without and with the adsorption of different gaseous molecules (CO, H_2S, NH_3, SO_2, CO_2, NO, and NO_2) on the surface of the CuBr ML are given in Table 2. The band gap of the pristine CuBr ML is 3.198 eV, which is in accordance with the previous DFT studies.[26]

The adsorption of combustible gases CO, H_2S and NH_3 does not change the semiconducting feature due to the large band gap after adsorption. In the case of CO, the band gap E_g is reduced to 3.050 eV as compared to the pristine CuBr ML. The CO molecule acts as a charge donor and after adsorption new peaks are noticed due to C-p and O-p orbitals of the CO molecule at about 1.988 eV in the conduction band (CB) near the Fermi level. The PDOS of CO adsorption shows strong hybridization of orbitals as shown in Fig. 6(a), which is due to the high value of the adsorption energy of the CO molecule. On the other hand, the H_2S and NH_3 adsorptions show small increases in the E_g values to 3.316 and 3.276 eV respectively. The H_2S and NH_3 adsorptions show strong adsorption energy values but still no significant difference is observed in the DOS of the combined CuBr after adsorption of these molecules and pristine CuBr ML close to the Fermi level, which implies the advantage and sensitivity of the CuBr ML for the adsorption of these combustible gases. A small contribution from the H_2S electronic states to the total DOS of the H_2S–CuBr system is localized in the valence band (VB), away from the Fermi level (about −2.924 eV) due to S-p orbitals as given in Fig. 6(b). The contribution of NH_3 electronic states to the total DOS of NH_3–CuBr is localized in the VB, near the Fermi level (about −1.675 eV) due to N-p orbitals as given in Fig. 6(c).

In the case of non-combustible HF gas molecule adsorption, it is observed that the energy band gap (E_g) is slightly reduced to 3.191 eV for the HF–CuBr system. The PDOS of HF adsorption plotted in Fig. 6(d), shows that CuBr after adsorbing HF keeps maintaining the semiconducting feature with a large band gap. The HF electronic levels' contribution to the overall DOS of the whole system is concentrated in the valence bands (VB), away from the Fermi level, at a location of −4.262 eV due to F-p orbitals. Near the Fermi level, however no major difference is observed between the DOS of the intrinsic CuBr ML and the HF–CuBr system. Also no strong hybridization of orbitals is observed in the PDOS because of the smaller adsorption energy of HF gas molecules.

In the case of adsorption of inert gases CO_2 and SO_2, a very small difference is observed in the band gap of the CuBr ML after adsorption of CO_2 molecule, whereas a significant decrease in band gap (1.536 eV) is observed in the case of SO_2 but keeping the semiconducting feature after adsorption in both cases. For CO_2, the electronic levels' contribution to the total DOS of the CO_2–CuBr system is localized in the VB, far from the Fermi level, at a location of about −4.938 eV due to O-p orbitals as shown in Fig. 6(e). Therefore close to the Fermi level, there is no notable variation between the DOS of the CO_2–CuBr and CuBr ML and no hybridization of orbitals is observed in the PDOS because of the smaller adsorption energy, indicating the physisorption phenomenon in CO_2 adsorption. The SO_2 electronic levels' contribution to the total DOS of the combined systems (SO_2–CuBr) is localized in the CB, close to the Fermi level, at a location of about 0.740 eV due to S-p and O-p orbitals as shown in Fig. 6(f).

Table 2 Band gap energy (E_g), sensitivity of the CuBr ML towards various gas molecules, work function (ϕ) and diffusion energy barrier (DEB) values of the pristine CuBr ML and with gas molecules adsorption. (↑/↓) shows spin up and spin down band gap

Model	E_g (eV)	Φ (eV)	DEB (eV)	Sensitivity
CuBr ML	3.198	4.21	—	—
CO–CuBr	3.050	4.77	1.51	16.50
H_2S–CuBr	3.316	4.38	0.62	0.90
NH_3–CuBr	3.276	4.98	0.91	0.78
HF–CuBr	3.191	5.13	0.014	0.14
SO_2–CuBr	1.536	4.64	0.44	9.12×10^{13}
CO_2–CuBr	3.193	4.39	0.81	0.10
NO–CuBr	0↑/1.92↓	5.56	0.55	7.28×10^{26}
NO_2–CuBr	2.06↑/0.11↓	5.17	1.02	3.62×10^{9}

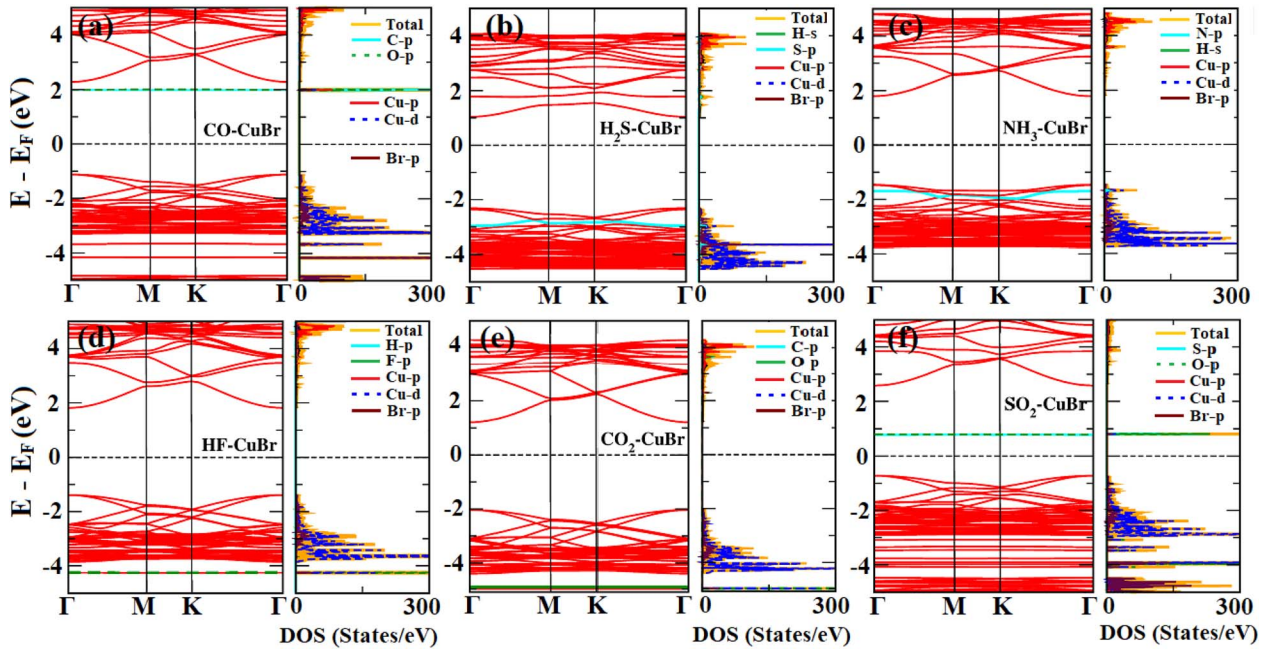

Fig. 6 The total and partial densities of states (PDOS) and band structures of (a) CO, (b) H_2S, (c) NH_3, (d) HF, (e) CO_2, (f) SO_2 adsorbed on the CuBr ML.

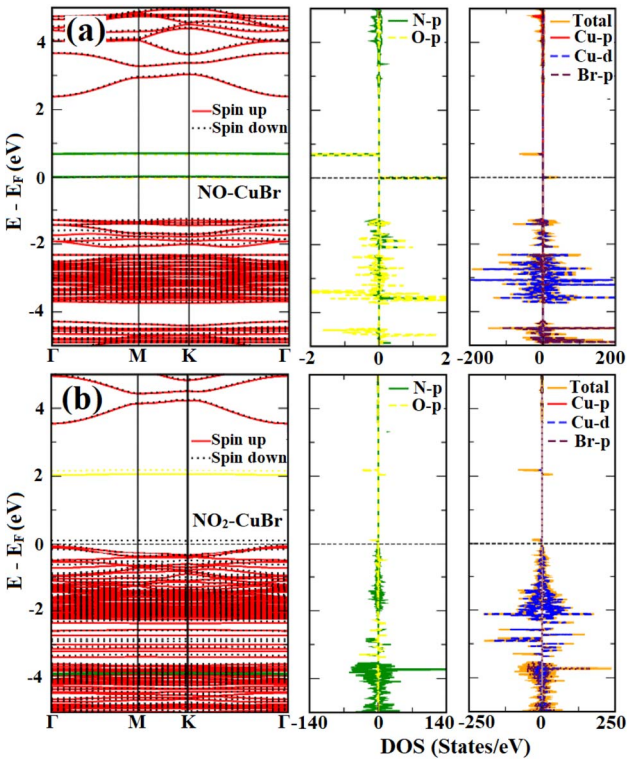

Fig. 7 The total and partial densities of states (PDOS) and band structures of paramagnetic (a) NO and (b) NO_2 molecules adsorbed on the CuBr ML.

In contrast, the oxidizer gases NO and NO_2 are paramagnetic and their adsorption introduces spin-polarization, due to which an asymmetry is introduced between the spin up/down (↑/↓) states. In Fig. 7(a) and (b), it is observed that a significant doping impact is produced by the spin-induced magnetic moment, where NO and NO_2 gas molecules act as charge acceptors with high values of charge transfer ($-0.528|e|$ and $-0.812|e|$) respectively. The magnetic moment could also be the major cause for the strong adsorption energy (-0.852 eV for NO, -1.754 eV for NO_2) and band gap reduction. For NO the band gap is reduced to 0.0 eV (spin up) and 1.92 eV (spin down) and for NO_2, the band gap is decreased to 2.06 eV (spin up) and 0.11 eV (spin down) upon adsorption of the NO_2 gas molecule on the CuBr monolayer.

Furthermore, the CDD is demonstrated to provide additional understanding of the transfer of charge between gas molecules and the CuBr ML. Eqn (3) is used to determine the CDD, and the resulting diagrams are shown in Fig. 8. The charge depletion is represented by the cyan region, and the charge gain is shown by the yellow region. For the combustible gases, the CO molecule acts as a charge acceptor. Whereas H_2S and NH_3 act as a charge donor with small charge transfer from these gas molecules to the CuBr ML showing the physisorption phenomenon in the case of these combustible gases. In the case of the non-combustible HF gas molecule adsorption, the charge is accumulated on the F of the HF molecule, indicating that the HF molecule behaves as a charge acceptor. It may be due to high electronegativity of the F atom. Here also a small charge is lost by the Br atom of the CuBr ML to the HF showing physisorption. In the case of inert gases SO_2 and CO_2, both the gas molecules behave as charge acceptors due to the high electronegativity of the oxygen atoms and charge is transferred from the CuBr ML to the molecule. In this case the charge accumulation is observed between two O atoms, and charge depletion is seen between Cu and Br atoms of the CuBr ML. For the adsorption of oxidizer

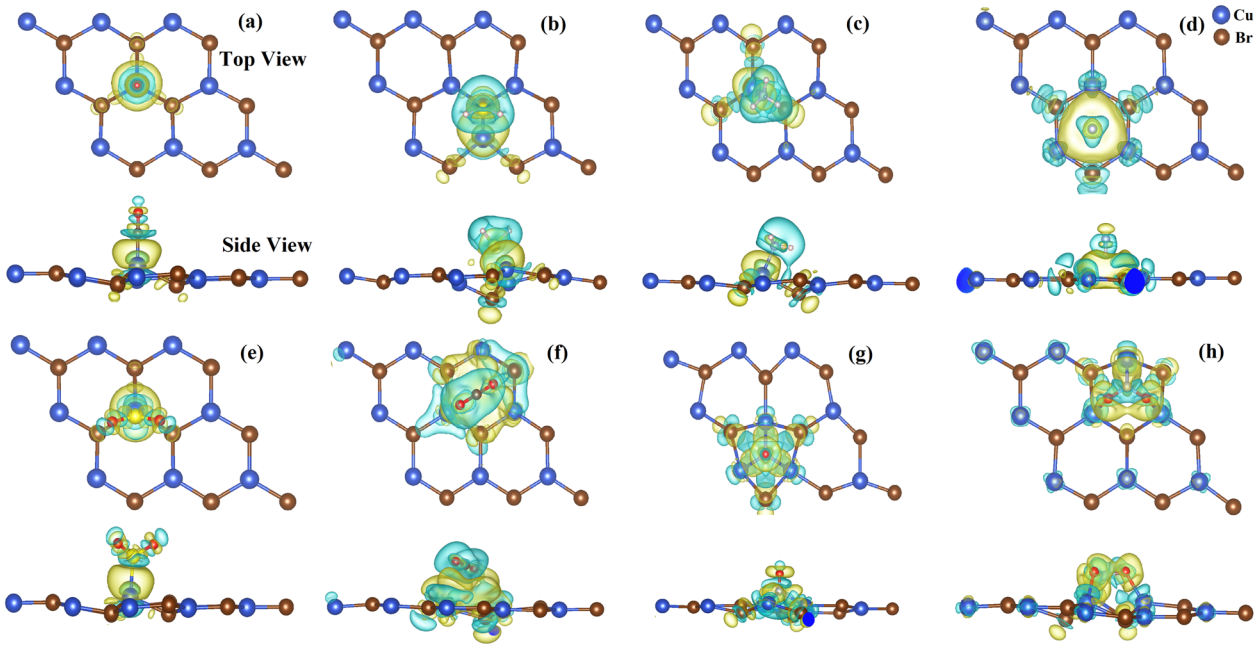

Fig. 8 Charge density difference (CDD) of (a) CO, (b) H_2S, (c) NH_3, (d) HF, (e) SO_2, (f) CO_2, (g) NO and (h) NO_2 adsorbed on the CuBr monolayer. Green, yellow, red, black, gray and orange balls represent H, F, O, C, S, and N atoms respectively.

gases NO and NO_2, charge accumulation is observed on the molecule side. This may be due to the electron-accepting nature of the N and O atoms of the NO and NO_2 molecules that show high values for their adsorption energy upon the CuBr ML. High values of charge transmission of $-0.582|e|$ and $-0.812|e|$ are observed from the CuBr ML to these molecules, indicating the chemisorption between NO/NO_2 and the CuBr ML.

In our research work, the calculation of the work function is done by using eqn (4), to further examine the impact of gas adsorption on the CuBr ML. It indicates the least energy needed to eliminate an electron from the ML surface. Work function is commonly used to assess a material's sensitivity when a gas sensor based on the Kelvin method is used and in this approach measurement of ϕ is done before and after gas exposure on sensing material using a Kelvin oscillator instrument.[59] Variations in ϕ during gas exposure would have an impact on the sensitivity of the sensor. The work function varies in response to variations in the charge concentration, so it is connected to conductivity. Fig. 9 shows the ϕ values of the CuBr ML without and with adsorption of the gas molecules. The work function of the pristine CuBr ML (4.21 eV) increases as a result of the adsorption of all gas molecules, suggesting that this adsorption is preventing electrons from moving to the vacuum level. Consequently, the work function can be greatly impacted by the adsorption of a specific gas molecule and the sensitivity of each molecule upon the CuBr ML depends on the percentage variations of ϕ (before and after adsorption), whose values in response to HF, CO, SO_2, NH_3, NO and NO_2 gas adsorptions are 21.8, 13.3, 10.2, 16.1, 32.0 and 22.8%. Therefore the CuBr ML is quite sensitive to all six of these gases, as evidenced by the variations in their work functions after adsorption.

The sensitivity and selectivity of a monolayer for specific gas molecules also depends on the variation of the band gap. Eqn (5) indicates that the conductivity is proportional to the exponential of band gap, which reflects that a change in the band gap width results in a change in the conductivity. The sensitivity of a monolayer for a molecule can be defined by the change in conductivity as given by eqn (6).[59] The calculated sensitivity of the CuBr ML towards different gas molecules is given in Table 2, which shows that SO_2, NO and NO_2 gas molecules have greater sensitivity due to the greater change in conductivity as compared to other gas molecules, and similarly the selectivity of these molecules depends on the percentage change in band gap whose values for HF, CO, CO_2, H_2S and NH_3 are small which indicates that the CuBr ML cannot distinguish between the sensing of these molecules. On the contrary, the variations in band gap for SO_2, NO and NO_2 are 52, 100↑/40↓ and 35.6 ↑/96.6↓% respectively. The (↑/↓) shows spin up and spin down band gaps. The results show that the CuBr ML is quite selective to these three gas molecules.

Application feasibility of a high performing and practically efficient gas sensor depends upon the fact that the gas adsorption mechanism must allow the gas to remain on the sensor surface long enough to be detected and then removed without damaging it. The gas molecule needs to stay adsorbed on the gas sensing material for the first instance at ambient temperature (300 K). When gas is successfully detected, the gas sensor should quickly return to its initial state. Table 3 shows the estimated recovery times with the exposure to visible light (attempt frequency $\nu_0 = 10^{12}$ s^{-1})[55] at different temperatures of 300 K, 400 K, and 500 K. Also for CO, NH_3 and NO_2 gas molecules the recovery time is calculated in the presence of UV light ($\nu_0 = 10^{15}$ s^{-1}).[37] We have examined the CuBr monolayer's room

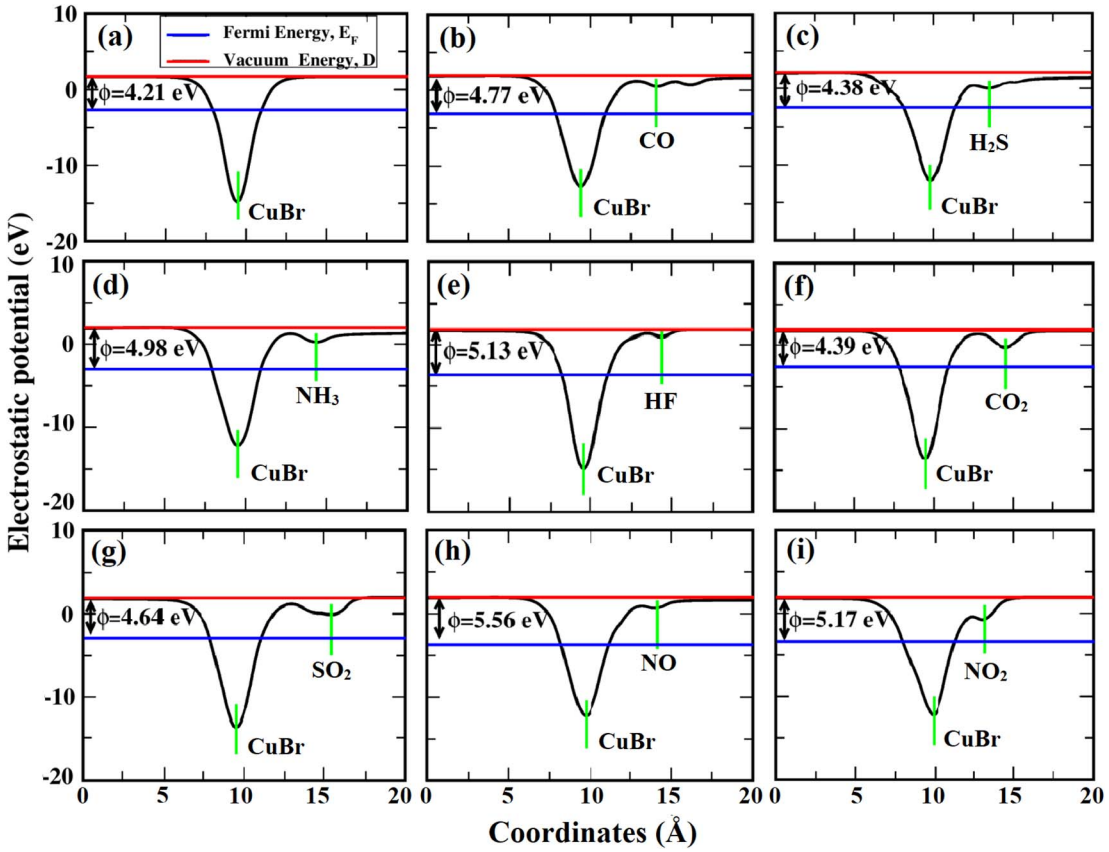

Fig. 9 Calculated work function of (a) CuBr-ML, (b) CO–CuBr, (c) H_2S–CuBr, (d) NH_3–CuBr, (e) HF–CuBr, (f) CO_2–CuBr, (g) SO_2–CuBr, (h) NO–CuBr and (i) NO_2–CuBr.

Table 3 Recovery time of the CuBr monolayer for HF, CO, CO_2, SO_2, H_2S, NH_3, NO and NO_2 gas desorption

	Recovery time (τ)			
Material	300 K Visible light	400 K Visible light	500 K Visible light	500 K UV light
CO	3.84×10^{9} s	1.55×10^{4} s	8.97 s	8.97×10^{-3} s
H_2S	4.71×10^{7} s	9.4 min	0.64 s	—
NH_3	7.00×10^{9} s	1.58×10^{4} s	9.38 s	9.38×10^{-3} s
HF	7.04×10^{-9} s	7.68×10^{-10} s	2.03×10^{-10} s	—
SO_2	3.95×10^{-2} s	8.86×10^{-5} s	2.35×10^{-6} s	—
CO_2	4.44×10^{-8} s	2.98×10^{-9} s	6.01×10^{-10} s	—
NO	3.23 min	5.44×10^{-2} s	3.86×10^{-4} s	—
NO_2	2.79×10^{17} s	1.15×10^{10} s	4.69×10^{5} s	7.81 min

temperature (300 K) gas sensing capability in order to confirm its feasibility for real-time applications. For determining the reusability of a gas sensor, its recovery time is calculated using eqn (7). The recovery period for HF, CO_2 and SO_2 is very small, therefore the CuBr ML can thus be utilized frequently for detection of these gas molecules at room temperature, since these gas molecules can be readily desorbed from the CuBr surface. The recovery time of H_2S and NO at 300 K is high, which can be further reduced by increasing the temperature. The full desorption of CO, NH_3 and NO_2 gas molecules from the CuBr ML at 500 K requires long recovery times. Eqn (7) indicates that if the adsorption energy E_{ads} is kept the same, then a shortened recovery time can be obtained by either a higher temperature or increasing attempt frequency (UV light exposure) or both because the UV light helps the sensor to recover quickly, therefore the recovery time of these gas molecules at a high temperature of 500 K in the presence of ultraviolet light can be reduced to an acceptable value. As a result the CuBr monolayer is predicted to be a promising material for gas sensing of HF, CO, CO_2, SO_2, H_2S, NH_3, NO and NO_2 gases.

4. Conclusion

In summary, the results obtained through first-principles calculations demonstrate that the CuBr monolayer (ML) shows different adsorption behaviors when exposed to common and contaminating gas molecules (HF, CO, CO_2, SO_2, H_2S, NH_3, NO and NO_2). The CuBr ML reveals a strong adsorption affinity for CO, SO_2, H_2S, NH_3, NO and NO_2 molecules as compared to HF and CO_2. The band structure and PDOS reveal that the electronic properties of the CuBr ML are altered due to the orbital contributions of the gas molecules (C-p and O-p of CO, F-p of HF, O-p of CO_2, S-p of H_2S, N-p of NH_3, S-p and O-p of SO_2, N-p and O-p of NO and NO_2) and the CuBr ML (Cu-p, Cu-d, Br-p) The gas molecules CO, CO_2, NH_3 and NO_2 have large DEB values

as compared to the other molecules. The CDD and Bader charge analysis indicate that the gas molecules act as charge acceptors or donors. The work function variation of the CuBr ML after adsorption and significant changes in the conductivity verify the sensitivity of these gas molecules. The percentage band gap variation for SO_2, NO and NO_2 is observed to be greater as compared to the other molecules showing that the CuBr monolayer is quite selective for these molecules. The recovery time for HF, CO_2 and SO_2 is very small at 300 K, therefore the CuBr ML can be utilized frequently for detection of these molecules at room temperature. However the recovery time for the other molecules can be significantly reduced by using high temperature with exposure to UV light. Thus our theoretical results indicate that monolayer CuBr is a promising candidate for gas sensing applications with high sensitivity and selectivity for CO, H_2S, NH_3, SO_2, NO and NO_2 gas molecules.

Data availability

The data supporting this article has been included as part of this manuscript.

Conflicts of interest

The authors declare that they have no known competing financial interests or personal relationships that could have appeared to influence the work reported in this paper.

Acknowledgements

The authors would like to thank the Researchers Supporting Project Number (RSP2025R511), King Saud University, Riyadh, Saudi Arabia. The author Y. Saeed would like to thank the Higher Education Commission (HEC) of Pakistan for providing a grant under NRPU-15844.

Notes and references

1 Z. Xie, F. Yang, X. Xu, R. Lin and L. Chen, *Front. Chem.*, 2018, **6**, 430.
2 K. Rasool, R. P. Pandey, P. A. Rasheed, S. Buczek, Y. Gogotsi and K. A. Mahmoud, *Mater. Today*, 2019, **30**, 80.
3 B. Wang, Y. Gu, L. Chen, L. Ji, H. Zhu and Q. Sun, *Nanotechnology*, 2022, **33**, 252001.
4 X. Xie and N. Zhang, *Adv. Funct. Mater.*, 2020, **30**, 2002528.
5 J. Pang, R. G. Mendes, A. Bachmatiuk, L. Zhao, H. Q. Ta, T. Gemming, H. Liu, Z. Liu and M. H. Rummeli, *Chem. Soc. Rev.*, 2019, **48**, 72.
6 H. Qin, C. Feng, X. Luan and D. Yang, *Nanoscale Res. Lett.*, 2018, **13**, 264.
7 B. Cho, M. G. Hahm, M. Choi, J. Yoon, A. R. Kim, Y.-J. Lee, S.-G. Park, J.-D. Kwon, C. S. Kim, M. Song, *et al.*, *Sci. Rep.*, 2015, **5**, 8052.
8 S.-Y. Cho, K.-H. Woo, J.-S. Kim, S.-Y. Yoon, J.-Y. Na, J.-H. Yu and Y.-B. Kim, *Ann. Occup. Environ. Med.*, 2013, **25**, 36.
9 N. Nasiri and C. Clarke, *Biosensors*, 2019, **9**, 43.
10 G. Panneerselvam, V. Thirumal and H. M. Pandya, *Arch. Acoust.*, 2018, **43**, 357.
11 K. S. Novoselov, D. Jiang, F. Schedin, T. Booth, V. Khotkevich, S. Morozov and A. K. Geim, *Proc. Natl. Acad. Sci. U. S. A.*, 2005, **102**, 10451.
12 H. Suzuki, N. Ogura, T. Kaneko and T. Kato, *Sci. Rep.*, 2018, **8**, 11819.
13 C. Chen, M. Wang, J. Wu, H. Fu, H. Yang, Z. Tian, T. Tu, H. Peng, Y. Sun, X. Xu, *et al.*, *Sci. Adv.*, 2018, **4**, eaat8355.
14 C. Shen and S. O. Oyadiji, *Mater. Today Phys.*, 2020, **15**, 100257.
15 A. P. Dral and J. E. ten Elshof, *Sens. Actuators, B*, 2018, **272**, 369.
16 R. Kumar, N. Goel, M. Hojamberdiev and M. Kumar, *Sens. Actuators, A*, 2020, **303**, 111875.
17 P. Bhattacharyya and D. Acharyya, *IEEE Sens. J.*, 2021, **21**, 22414.
18 H. Mi, Q. Zhou and W. Zeng, *Appl. Surf. Sci.*, 2021, **563**, 150329.
19 X. Zhang, Z. Lai, C. Tan and H. Zhang, *Angew. Chem., Int. Ed.*, 2016, **55**, 8816.
20 E. Lee and D.-J. Kim, *J. Electrochem. Soc.*, 2020, **167**, 037515.
21 S. Sinha, Y. Takabayashi, H. Shinohara and R. Kitaura, *2D Mater.*, 2016, **3**, 035010.
22 M. S. Khan, A. Srivastava and R. Pandey, *RSC Adv.*, 2016, **6**, 72634.
23 J. Wu, Y. Wei, W. Shen, Y. Xiong, C. Lin, Y. Gao, A. AL-Ammari, K. Liu, T. Ma, J. Chen, *et al.*, *Appl. Phys. Lett.*, 2020, **116**, 261903.
24 C. Gong, J. Chu, C. Yin, C. Yan, X. Hu, S. Qian, Y. Hu, K. Hu, J. Huang, H. Wang, *et al.*, *Adv. Mater.*, 2019, **31**, 1903580.
25 M. Altarawneh, A. Marashdeh and B. Z. Dlugogorski, *Phys. Chem. Chem. Phys.*, 2015, **17**, 9341.
26 X. Huang, L. Yan, Y. Zhou, Y. Wang, H.-Z. Song and L. Zhou, *J. Phys. Chem. Lett.*, 2021, **12**, 525.
27 R. Zacharia, H. Ulbricht and T. Hertel, *Phys. Rev. B: Condens. Matter Mater. Phys.*, 2004, **69**, 155406.
28 H. Liu, A. T. Neal, Z. Zhu, Z. Luo, X. Xu, D. Tománek and P. D. Ye, *ACS Nano*, 2014, **8**, 4033.
29 Y. Cai, G. Zhang and Y.-W. Zhang, *J. Am. Chem. Soc.*, 2014, **136**, 6269.
30 S. Bruzzone and G. Fiori, *Appl. Phys. Lett.*, 2011, **99**, 222108.
31 S. Pervaiz, M. U. Saeed, S. Khan, B. Asghar, Y. Saeed, H. O. Elansary and A. Bacha, *RSC Adv.*, 2024, **14**, 16284.
32 X. Sun, Q. Yang, R. Meng, C. Tan, Q. Liang, J. Jiang, H. Ye and X. Chen, *Appl. Surf. Sci.*, 2017, **404**, 291.
33 L. Kou, T. Frauenheim and C. Chen, *J. Phys. Chem. Lett.*, 2014, **5**, 2675.
34 B. Zhu, K. Zheng, X. Chen, J. Qiu, H. Guo, F. Zhang, L. Lang, J. Yu and J. Bao, *Phys. Chem. Chem. Phys.*, 2021, **23**, 1675.
35 Y.-H. Zhang, Y.-B. Chen, K.-G. Zhou, C.-H. Liu, J. Zeng, H.-L. Zhang and Y. Peng, *Nanotechnology*, 2009, **20**, 185504.
36 L. Chhana, B. Lalroliana, R. C. Tiwari, B. Chettri, L. Pachuau, S. Gurung, L. Vanchhawng, D. P. Rai, L. Zuala and R. Madaka, *ACS Omega*, 2022, **7**, 40176.
37 B. A. Kalwar, W. Fangzong, A. M. Soomro, M. R. Naich, M. H. Saeed and I. Ahmed, *RSC Adv.*, 2022, **12**, 34185.

38 V. Babar, H. Vovusha and U. Schwingenschlögl, *ACS Appl. Nano Mater.*, 2019, **2**, 6076.
39 A. Bafekry, M. Faraji, M. Fadlallah, A. A. Ziabari, A. B. Khatibani, S. Feghhi, M. Ghergherehchi and D. Gogova, *Appl. Surf. Sci.*, 2021, **564**, 150326.
40 N. Tit, K. Said, N. M. Mahmoud, S. Kouser and Z. H. Yamani, *Appl. Surf. Sci.*, 2017, **394**, 219.
41 X.-f. Yu, Y.-c. Li, J.-b. Cheng, Z.-b. Liu, Q.-z. Li, W.-z. Li, X. Yang and B. Xiao, *ACS Appl. Mater. Interfaces*, 2015, **7**, 13707.
42 X.-P. Chen, L.-M. Wang, X. Sun, R.-S. Meng, J. Xiao, H.-Y. Ye and G.-Q. Zhang, *IEEE Electron Device Lett.*, 2017, **38**, 661.
43 Z. Xu, Z. Shi, M. Wang, R. Song, X. Zhang, G. Liu and G. Qiao, *Sens. Actuators, A*, 2021, **328**, 112766.
44 P. Giannozzi, S. Baroni, N. Bonini, M. Calandra, R. Car, C. Cavazzoni, D. Ceresoli, G. L. Chiarotti, M. Cococcioni, I. Dabo, *et al.*, *J. Phys.: Condens. Matter*, 2009, **21**, 395502.
45 J. P. Perdew, K. Burke and M. Ernzerhof, *Phys. Rev. Lett.*, 1996, **77**, 3865.
46 D. Vanderbilt, *Phys. Rev. B: Condens. Matter Mater. Phys.*, 1990, **41**, 7892.
47 S. Grimme, *J. Comput. Chem.*, 2006, **27**, 1787.
48 U. Khan, M. U. Saeed, H. O. Elansary, I. M. Moussa, Y. Saeed, *et al.*, *RSC Adv.*, 2024, **14**, 4844.
49 F. A. Khan, M. U. Saeed, U. Khan, H. O. Elansary, A. Z. Dewidar, Y. Saeed, *et al.*, *Solid State Sci.*, 2024, **153**, 107554.
50 Z. Ali, A. Razzaq, S. M. Ali, M. U. Saeed, H. O. Elansary, I. M. Moussa, M. A. El-Sheikh, A. U. R. Bacha and Y. Saeed, *J. Electron. Mater.*, 2024, **53**, 3834.
51 S. M. Ali, M. U. Saeed, H. O. Elansary and Y. Saeed, *RSC Adv.*, 2024, **14**, 3178.
52 H. J. Kulik, M. Cococcioni, D. A. Scherlis, and N. Marzari, *arXiv*, 2006, preprint, arXiv:cond-mat/0608285, DOI: **10.48550/arXiv.cond-mat/0608285**.
53 H. J. Monkhorst and J. D. Pack, *Phys. Rev. B*, 1976, **13**, 5188.
54 G. Henkelman, A. Arnaldsson and H. Jónsson, *Comput. Mater. Sci.*, 2006, **36**, 354.
55 R. Shahriar, O. Hassan and M. K. Alam, *RSC Adv.*, 2022, **12**, 16732.
56 V. Mehta, H. S. Saini, S. Srivastava, M. K. Kashyap and K. Tankeshwar, *J. Phys. Chem. C*, 2019, **123**, 25052.
57 V. Mehta, H. S. Saini, S. Srivastava, M. K. Kashyap and K. Tankeshwar, *Mater. Today Commun.*, 2021, **26**, 102100.
58 A. Sengupta, *Appl. Surf. Sci.*, 2018, **451**, 141.
59 D. Chidambaram, R. Kalidoss, K. Pushparaj, V. J. Surya and Y. Sivalingam, *Mater. Sci. Eng., B*, 2022, **280**, 115694.